

Attempt to Adapt Sault-Wieringa Deconvolution to High Dynamic Range Imaging

W. D. Cotton and F. R. Schwab, February 25, 2010

Abstract—This memo describes an attempt to adapt the wide-band deconvolution technique of Sault and Wieringa to high dynamic range imaging. The method is also extended to include a second order term. This approach works very well for point sources but is not significantly better than conventional techniques for extended sources.

Index Terms—Wide-band Imaging, Interferometry

I. INTRODUCTION

ONE of the principle ways in which radio interferometer arrays presently under construction or in planning increase their sensitivities over current arrays is by a large increase in the bandwidth being sampled. This presents challenges to imaging the data from the new arrays as the large bandwidths violate one of the implicit assumption used in imaging, that the sky looks the same at all frequencies in the observed bandpass. This assumption can be relaxed somewhat by assuming that all the emission in the image has the same spectral shape – but with a sufficiently wide bandpass and a range of spectral shapes in the primary antenna pattern, this assumption breaks down.

To reach the sensitivity which the new instruments are in theory capable of, all of the sky in which there are detectable sources must be imaged in order to remove the side-lobes of these sources. At lower frequencies this essentially means that the entire primary beam must be imaged along with selected areas in the side-lobes. Thus, especially at lower frequencies, a wide-band imaging problem is also a wide-field imaging problem. This increases the likelihood of a range of spectral shapes in the image.

This memo describes a follow up to the work described in [1] but using an attempt to adapt the technique of Sault and Wieringa [2], [3] to high dynamic range imaging. This development used the Obit ([4], <http://www.cv.nrao.edu/~bcotton/Obit.html>) package.

II. THE SAULT-WIERINGA TECHNIQUE

The technique of Sault and Wieringa [2] is to develop a linear decomposition of the spectral imaging problem into a sum of image spectral terms and beams describing the image response to the various spectral terms. They present a solution involving the convolutions of the image residuals with the various beams and among the beams. As described, the technique solves for flux density and the derivative of flux

density with frequency for each image pixel using a Högbom CLEAN [5].

The Sault–Wieringa technique for a point source at position j is to find parameters a_0 and a_1 that minimize

$$\epsilon^2 = \sum_i (R(i) - a_0 B_0(i-j) - a_1 B_1(i-j))^2 \quad (1)$$

where B_0 and B_1 are “beams” that describe the contribution to the residuals, R , of the parameters a_0 and a_1 . A one dimensional representation of the image is used. The image parameters are obtained from the solution to the matrix equation:

$$\begin{bmatrix} R_0(j) \\ R_1(j) \end{bmatrix} = \begin{bmatrix} A_{00}(0) & A_{01}(0) \\ A_{10}(0) & A_{11}(0) \end{bmatrix} \begin{bmatrix} a_0 \\ a_1 \end{bmatrix} \quad (2)$$

where R_i is the convolution of the residual image with B_i , and A_{ij} is the convolution of B_i with B_j . When implemented in a CLEAN deconvolution, the most significant pixel, j , is the one that maximizes:

$$R_0(j)^2 A_{11}(0) + R_1(j)^2 A_{00}(0) - 2R_0(j)R_1(j)A_{01}(0) \quad (3)$$

(their eq. 22). For loop gain g , the residuals R_0 and R_1 are updated by:

$$\begin{aligned} R_0(i) - &= g(a_0 A_{00}(i-j) - a_1 A_{10}(i-j)) \\ R_1(i) - &= g(a_0 A_{01}(i-j) - a_1 A_{11}(i-j)) \end{aligned} \quad (4)$$

where the symbol “–=” denotes subtraction from.

III. EXTENDING THE SAULT-WIERINGA TECHNIQUE

There are a number of reasons for extending this technique. First, for very wide-band systems using the derivative of flux density with frequency will be an inadequate representation of sources whose spectra are generally well represented by a power law, possibly with some curvature. A significant curvature adds the requirement for a higher order representation as well. Finally, the Högbom CLEAN technique limits the dynamic range of images and some variation on the source estimation and subtraction from the visibility data (e.g. “Cotton-Schwab” CLEAN of [6], [7]) is needed to obtain high dynamic range images.

A. Spectral Representation

Astrophysical sources of broadband emission generally emit by either thermal or synchrotron mechanisms. In either case, the spectral shape over large areas of the radio spectrum are close to a power law. This suggests the form of the spectrum to

be assumed. The technique presented here uses the following adaptation of the traditional representation of a continuum source spectrum:

$$s_\nu = s_{\nu_0} e^{\alpha \log(\nu/\nu_0) + \beta \log(\nu/\nu_0)^2 + \dots} \quad (5)$$

where s is the spectral flux density, ν is frequency, ν_0 a reference frequency and α, β, \dots are the ‘‘spectral index’’ and one or more curvature terms. As many terms can be used in the exponent as are needed to accurately represent the observed emission. This is the same as the traditional scalar pixel representation with the addition of the exponential term to give the spectral shape.

Equation (5) is not a linear equation as needed by the Sault–Wieringa technique, however a first order Taylor series expansion is the same within 5% over a factor of two bandwidth and is represented by

$$S_\nu = S_0 + S_0 \alpha \ln\left(\frac{\nu}{\nu_0}\right) + S_0 \beta \left[\ln\left(\frac{\nu}{\nu_0}\right)\right]^2 \quad (6)$$

The Sault–Wieringa method can then be applied to parameters $S_0, S_0 \alpha$ and $S_0 \beta$.

The beams needed for the spectral decomposition are derived by replacing the data in the gridding with (1,0) for B_0 , $\left(\ln\left(\frac{\nu}{\nu_0}\right), 0\right)$ for B_1 and $\left(\left[\ln\left(\frac{\nu}{\nu_0}\right)\right]^2, 0\right)$ for B_2 .

B. Extension to Second Order

The extension of equations 2–4 to second order is straightforward; adding a third parameter, a_2 and its beam B_2 , equation (2) becomes:

$$\begin{bmatrix} R_0(j) \\ R_1(j) \\ R_2(j) \end{bmatrix} = \begin{bmatrix} A_{00}(0) & A_{01}(0) & A_{02}(0) \\ A_{10}(0) & A_{11}(0) & A_{12}(0) \\ A_{20}(0) & A_{21}(0) & A_{22}(0) \end{bmatrix} \begin{bmatrix} a_0 \\ a_1 \\ a_3 \end{bmatrix} \quad (7)$$

The equivalent of eq (3) (S&W eq 22) is :

$$\begin{aligned} & A_{12}(0)^2 R_0(j)^2 + (A_{02}(0)^2 - A_{00}(0)A_{22}(0))R_1(j)^2 \\ & \quad + A_{01}(0)^2 R_2(j)^2 + \\ & 2A_{01}(0)R_1(j)(A_{22}(0)R_0(j) - A_{02}(0)R_2(j)) - \\ & \quad 2A_{12}(0)(A_{02}(0)R_0(j)R_1(j) + \\ & \quad (A_{01}(0)R_0(j) - A_{00}(0)R_1(j))R_2(j)) - \\ & \quad A_{11}(0)(A_{22}(0)R_0(j))^2 + \\ & R_2(j)(-2A_{02}(0)R_0(j) + A_{00}(0)R_2(j)) \end{aligned} \quad (8)$$

For loop gain g , the residuals R_0, R_1 and R_2 are updated by eq (9):

$$\begin{aligned} R_0(i) & - = g(a_0 A_{00}(i-j) - a_1 A_{10}(i-j) - a_2 A_{20}(i-j)) \\ R_1(i) & - = g(a_0 A_{01}(i-j) - a_1 A_{11}(i-j) - a_2 A_{21}(i-j)) \\ R_2(i) & - = g(a_0 A_{02}(i-j) - a_1 A_{12}(i-j) - a_2 A_{22}(i-j)) \end{aligned}$$

C. High Dynamic range CLEAN

A visibility subtraction based CLEAN can be adapted to using the Sault–Wieringa technique by replacing the inner Clark CLEAN with one that estimates the one to three parameters needed for the spectral representation of the components. The CLEAN components then contain S_0, α and β as appropriate. The subtraction of these components from the visibility data

should calculate the value at each frequency as described in [1]. Since the inner component finding loop uses only an approximation of the spectral representation, the subtraction to determine accurate residuals should be done fairly often.

IV. OBIT IMPLEMENTATION

In Obit the Sault–Wieringa technique was implemented in the ObitDConCleanVis class using a number of derived subclasses. Storing the spectral information on the CLEAN components made use of modifications described in [1] and generally supported in the Obit SkyModel classes. Solutions to equations (2) and (7) are used to calculate the residual (S_0) image used to make the decisions about convergence etc. The derived specialized classes are described in the following:

• ObitDConCleanVisWB

Derived from ObitDConCleanVis and does the specialized operations:

- Fills and passes ObitFArrays with the various convolutions of residuals and beams. The Beam patch is always the full size of beam
- Decides which order of imaging is to be applied based on the user requests and the current state of the deconvolution.
- Uses ObitImageWB functions to decompose residuals into spectral components when residual images are made and to compute the various convolutions.
- Restores all spectral components to residuals, this uses flux weighted spectral components for α and β . Final normalization uses ObitDConCleanVisWB-SpecNorm.

• ObitDConCleanPxListWB

Derived from ObitDConCleanPxList, this is where the basic component finding is done. This class is given the various convolutions of beams and residuals and implements the basic Sault–Wieringa technique writing CLEAN components with the spectral information.

• ObitImageMosaicWB

Derived from ObitImageMosaic this class contains the images needed to cover the facets and outlying fields. When the mosaic is created or extended, the created images and beams are of type ObitImageWB. Images are doubled in size and unboxes are added to prevent placing CLEAN components into the outer portions of the images.

• ObitImageWB

Derived from ObitImage, objects of this class have a frequency–like axis with label SPECLOGF to indicate that the multiple planes are a spectral expansion in $\ln(\nu)$. This class also performs the convolutions of the residuals and beams as well as the decomposition of the residual images into spectral components. Normalizing all convolutions by the value of $A_{00}(0)$ puts the residuals in units of Jy.

• ObitUVImagerWB

Derived from ObitUVImager, this class creates ObitImageWBs from UV data. The chief difference is that the multiple beams (B_0, B_1 and B_2) are also formed.

- **ObitUVGridWB**

Derived from ObitUVGrid this grids UV data. The chief difference is that the multiple beams (B_0 , B_1 and B_2) are also formed.

The user interface is implemented via task SWImag. In addition to the usual Obit imaging task parameters are the following

- **norder**

This specifies the maximum order of imaging to be used; 0=only S_0 , 1= $S_0 + \alpha$, 2= $S_0 + \alpha + \beta$

- **OrdFlux**

This parameter is a set of residual levels causing the subsequent order of imaging to drop to the next lowest level.

One of the normal imaging parameters, ccfLim, has an increased importance. This limits the inner CLEAN cycle to residuals no smaller than ccfLim times the maximum residual that major cycle.

Because the result of the CLEAN is a set of CLEAN components with spectral information, all the usual self-calibration facilities are also available.

V. TESTS

A number of tests were performed to assure that the software was behaving properly and to evaluate the characteristics of the technique. For this a number of simulated datasets were developed from a range of models.

A. Model Data

Various model wide-band datasets were derived from a 15×390 kHz channel VLA dataset at 1.4 GHz with 1 “IF” involving multiple snapshots. This dataset was expanded to 10 IFs spaced at 100 MHz intervals which (sparsely) covers the range 1.4 to 2.3 GHz. The data values were replaced by the Fourier transform of one of the models described below. The flux density of each model was calculated from the spectral parameters for each channel.

B. Models

A number of source models were used ranging from a point source at the origin with a straight spectrum to a complex model with components of a wide range of sizes, shapes, flux densities and spectra. These are described in the following:

- 1) Point source with a straight spectrum at the origin. This model has 1.0 Jy and a spectral index (α) of -0.70.
- 2) Point source with a curved spectrum at the origin. This model has 1.0 Jy and a spectral index of -0.70 and curvature (β) of -0.2.
- 3) Extended source with a straight spectrum at the origin. This model has 0.5 Jy, a spectral index of -0.55 and is a $15'' \times 3''$ Gaussian with position angle of the major axis of -30° .
- 4) Extended source with a curved spectrum offset from the origin. This model has 4.0 Jy and consists of a $5'' \times 5''$ Gaussian offset by $69''$ in RA and $68''$ in Dec from the

TABLE I
“Multi” Model Parameters

	X ''	Y ''	S Jy	α	β	Maj ''	min ''	PA °
A	-50.0	50.0	0.001	0.0	0.0	0.0	0.0	
B	-50.0	-20.0	0.0002	0.0	0.0	0.0	0.0	
C	-36.0	-53.0	2.0	-0.75	-0.01	15.0	3.0	90.0
D	-15.0	-52.0	1.0	0.25	0.0	0.0	0.0	
E	-12.0	2.0	5.0	-1.25	-0.033	7.0	4.0	135.0
F	0.0	0.0	1.5	0.0	0.0	0.0	0.0	
G	4.0	-51.0	2.5	-0.65	-0.05	16.0	3.0	90.0
H	6.0	71.0	3.5	0.25	-0.15	0.0	0.0	
I	28.0	28.0	1.0	0.0	-0.0	1.0	1.0	
J	38.0	-12.0	3.0	-0.55	-0.025	20.0	5.0	15.0
K	69.0	68.0	4.0	-0.05	-0.1	5.0	5.0	

origin. The spectral index is -0.05 and a curvature of -0.1; this is also component K in Table I

- 5) Double source with straight spectra. The first component is a point at the origin with 1.0 Jy and a spectral index of -0.7. The second is a $15'' \times 3''$ Gaussian with position angle of the major axis of -30° offset from the origin by $30''$ in RA and Dec and has a spectral index of -0.55. This model is model 1 with model 3 offset from the center.
- 6) Complex “Multi” model. This consists of 11 point or Gaussian components with a variety of sizes, shapes, strengths and spectra. These are listed in Table I. The columns in this Table are: component label, RA offset, declination offset, flux density, spectral index, curvature, Gaussian major axis FWHM, Gaussian minor axis, and Gaussian position angle. The models include a range of flux densities, sizes, shapes and spectra. A small amount of zero mean Gaussian pseudo noise was added.

The “Multi” model image as derived from a traditional imaging ignoring spectral properties and a spectrally sensitive rendition are shown in Figure 1.

Since the datasets all used the same uv coverage, all had the same sets of beams. These beams are shown in Figure 2. The fitted restoring beam for all tests was $2.8'' \times 2.7''$ with position angle 32°

C. Test Results

The tests are summarized in Table II.

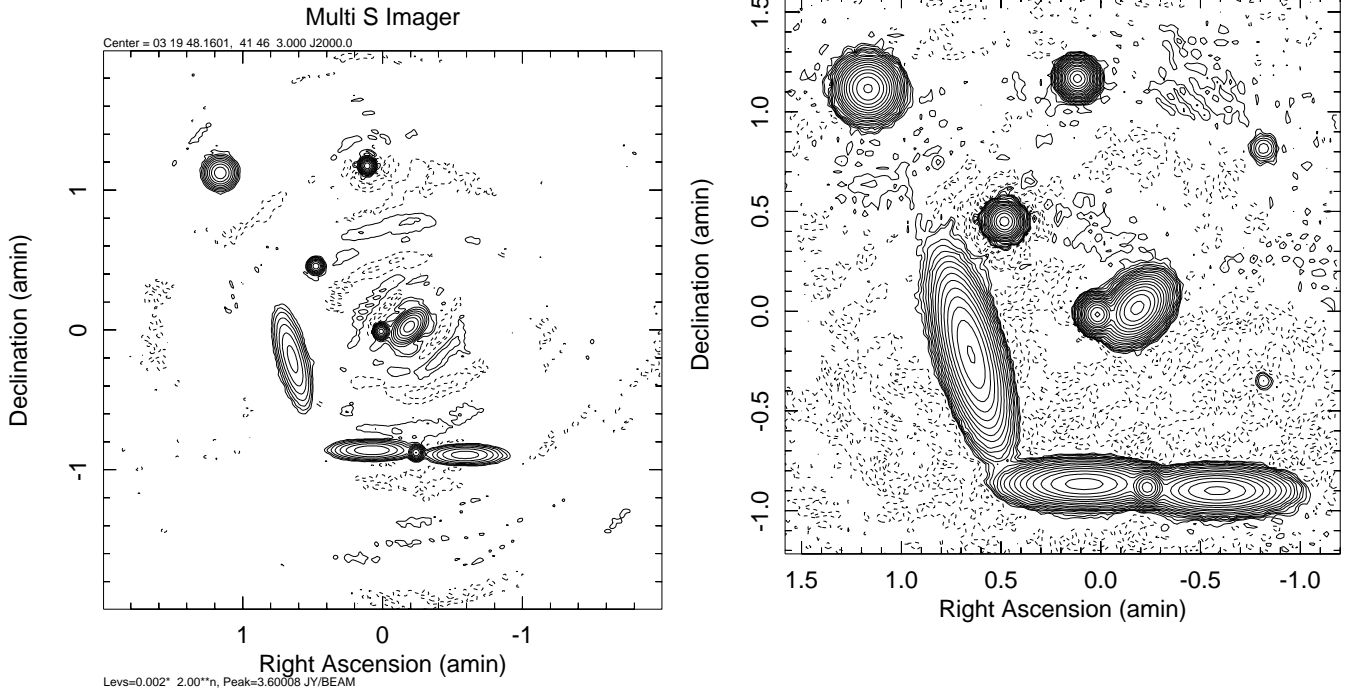


Fig. 1. **Left:** Multiple component model given in Table I with added noise. The image RMS is 0.94 mJy/bm and dynamic range is 3.8×10^3 . Contour levels are powers of 2 from 2 mJy/bm, the peak in the image is 3.6 Jy/beam. Negative contours are dashed. **Right:** Spectral fitting s_{ν_0} results from [1]. The image RMS is 0.014 mJy/bm and the dynamic range is 2.8×10^5 . Contouring uses levels spaced by powers of 2.0 from 2.0×10^{-2} mJy/beam, one hundred times lower than on **Left**. Resolution is that of the lowest frequency.

VI. DISCUSSION

The results on the testing using the various models is described in the following sections. In all tests the fields imaged were substantially larger than needed to cover the model used, even including the needed guard-bands for the convolutions. Smaller fields of view yielded poorer performance.

A. Model 1

This model is a point at the origin with a straight spectrum with $\alpha = -0.7$. The first test (Figure 3 top left) is to verify the non spectral portions of the software. Only the total intensity was solved for but the data were initially corrected for a spectral index of -0.7 . As expected, the result is excellent with a peak very close to 1.0 Jy and a dynamic range¹ of 5.1×10^8 . The off-source contours in this figure are mostly the result of the limited precision of the calculations.

The second test (Figure 3 top right) is similar to the first except that no correction was made to the data. As expected, the results of ignoring the model spectrum are poor. The peak in the image is only 0.82 Jy and the dynamic range was 3.3×10^3 .

The third test for Model 1 (Figure 3 bottom left) was solving for flux density and spectral index. The results are very good, the peak flux density was very close to 1.0 Jy, the peak α was -0.702 and the dynamic range was 5.0×10^6 .

The final test for Model 1 (Figure 3 bottom right) was to image solving for flux, α and β ; the β in the model was 0.

¹Dynamic range in this memo is defined as the ratio of the image peak to off source RMS

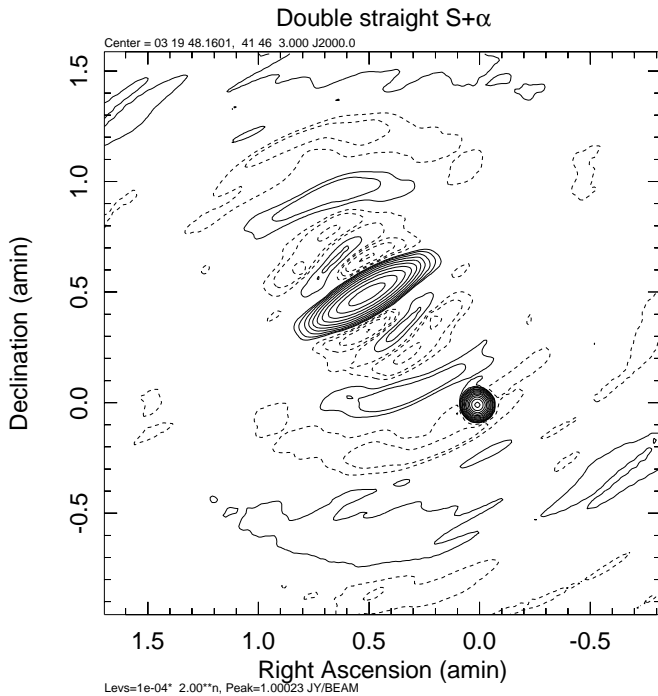


Fig. 7. Model 5. Imaged with $norder=1$ for all; 1839 CC Sum = 1.57689 Jy, resid = 3.4×10^{-4} , 3.7×10^{-4} , RMS = 6.3×10^{-5} , DR = 1.6×10^4 , center pt flux = 1.000227, $\alpha = -0.7038$, center extd flux = 0.0752, $\alpha = -1.71$ DR = 1.2×10^3 . Contour levels are powers of 2 from 0.1 mJy/beam, the peak in the image is 1.0 Jy/beam.

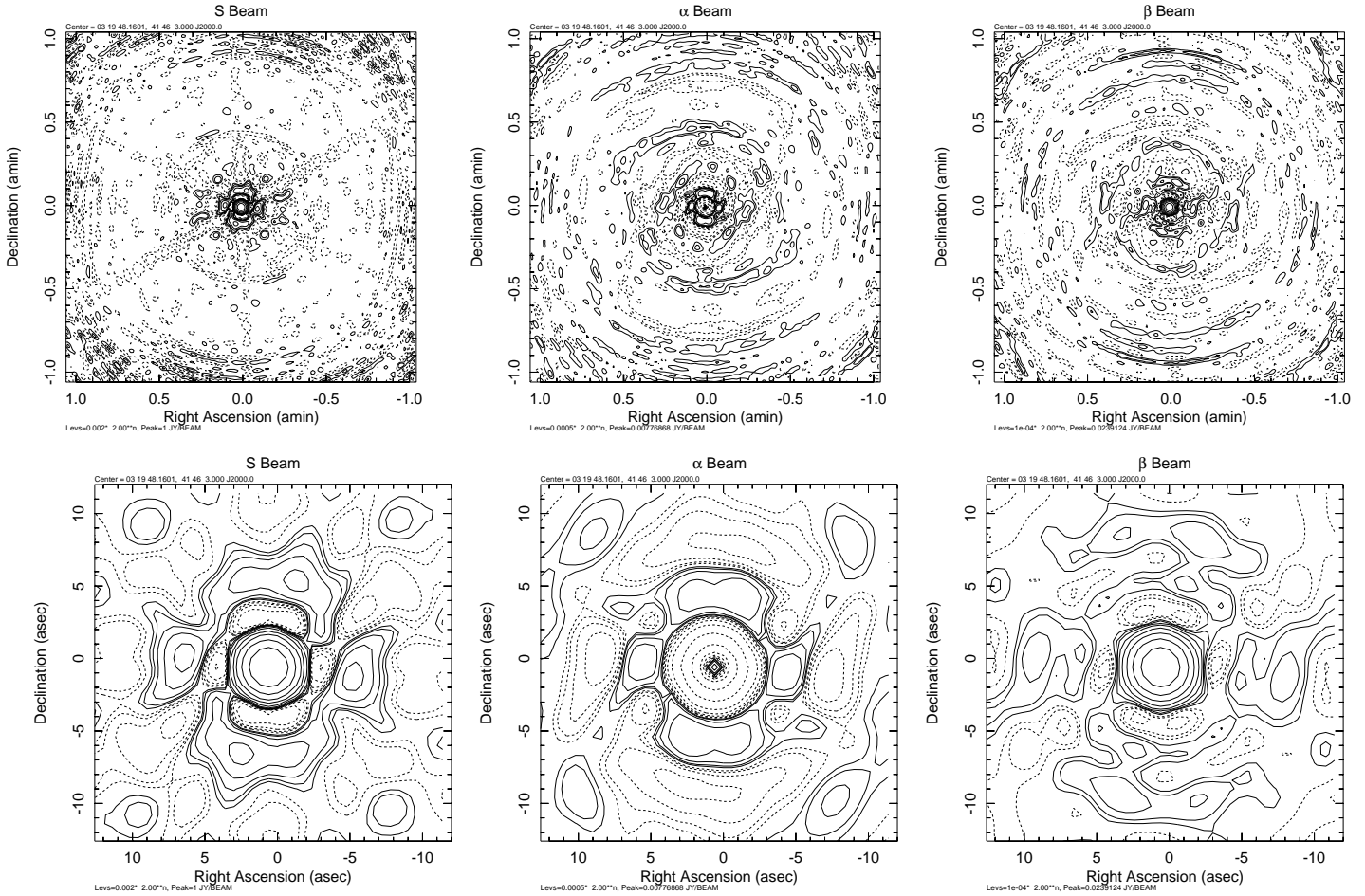


Fig. 2. **Top Left:** S (dirty) beam. Max and min values are 1.00 and -0.035; contours are powers of 2 from 0.002, Negative contours are dashed. **Top Center:** α beam. Max and min values are 0.0078 and -0.019; contours are powers of 2 from 5.0×10^{-4} . **Top Right:** β beam. Max and min values are 0.024 and -0.00054; contours are powers of 2 from 1.0×10^{-4} . **Bottom:** Central regions of the beams above.

Again, the results were very good, the peak was close to 1.0 Jy, the peak α was -0.696, β was -0.013 and the dynamic range 8.3×10^5 .

Both of the tests solving for the spectral properties of Model 1 yielded results very close to the input model and very good dynamic range.

B. Model 2

This model is also a point source but one with a curved spectrum; $S=1.0$, $\alpha=-0.70$, $\beta=-0.2$. The first test on Model 2 (Figure 4 left) was without solving for the spectrum and yields the expected poor result, The peak was 0.81 Jy and the dynamic range was 2.7×10^3 .

The second test for this model (Figure 4 right) was solving for flux, α and β . Here, the results are excellent, the peak flux density is very close to 1.0, $\alpha=0.700$, $\beta=-0.201$ and the dynamic range was 7.8×10^7 . The technique produces excellent results for point sources.

C. Model 3

This model was an extended source at the origin with a straight spectrum ($\alpha = -0.55$) and was a 0.5 Jy Gaussian of

$13'' \times 3''$ (beam size was $2.7''$). The first test for this model (Figure 5 upper left) was solving for only the flux density and ignoring the spectrum. Poor results were obtained as expected; the total flux density was 0.434 Jy and the dynamic range of 1.4×10^3 .

The second test (Figure 5 upper right) solved for both flux density and spectral index. The results were unexpectedly poor; the sum of the CLEAN components was 0.555 Jy, the α at the peak intensity was -1.81 and the dynamic range was 2.0×10^3 . This results was only marginally better than ignoring the spectrum and produces a spectral index very much steeper than the model.

To test if the poor imaging in the previous test was the results of the solution for spectral parameters becoming unstable well into the CLEAN, as they were observed to do, the third test (Figure 5 bottom) used the SWImag feature of reducing the order of the solution from solving for α to only flux density below 0.01 Jy. This resulted in 0.357 Jy being CLEANed modeling both flux and α and the remainder of the 0.547 Jy solving only for flux density. This yielded an image worse than the previous. The sum of the CLEAN flux densities was 0.555, the α at the peak was -1.74 and dynamic range 1.8×10^3 .

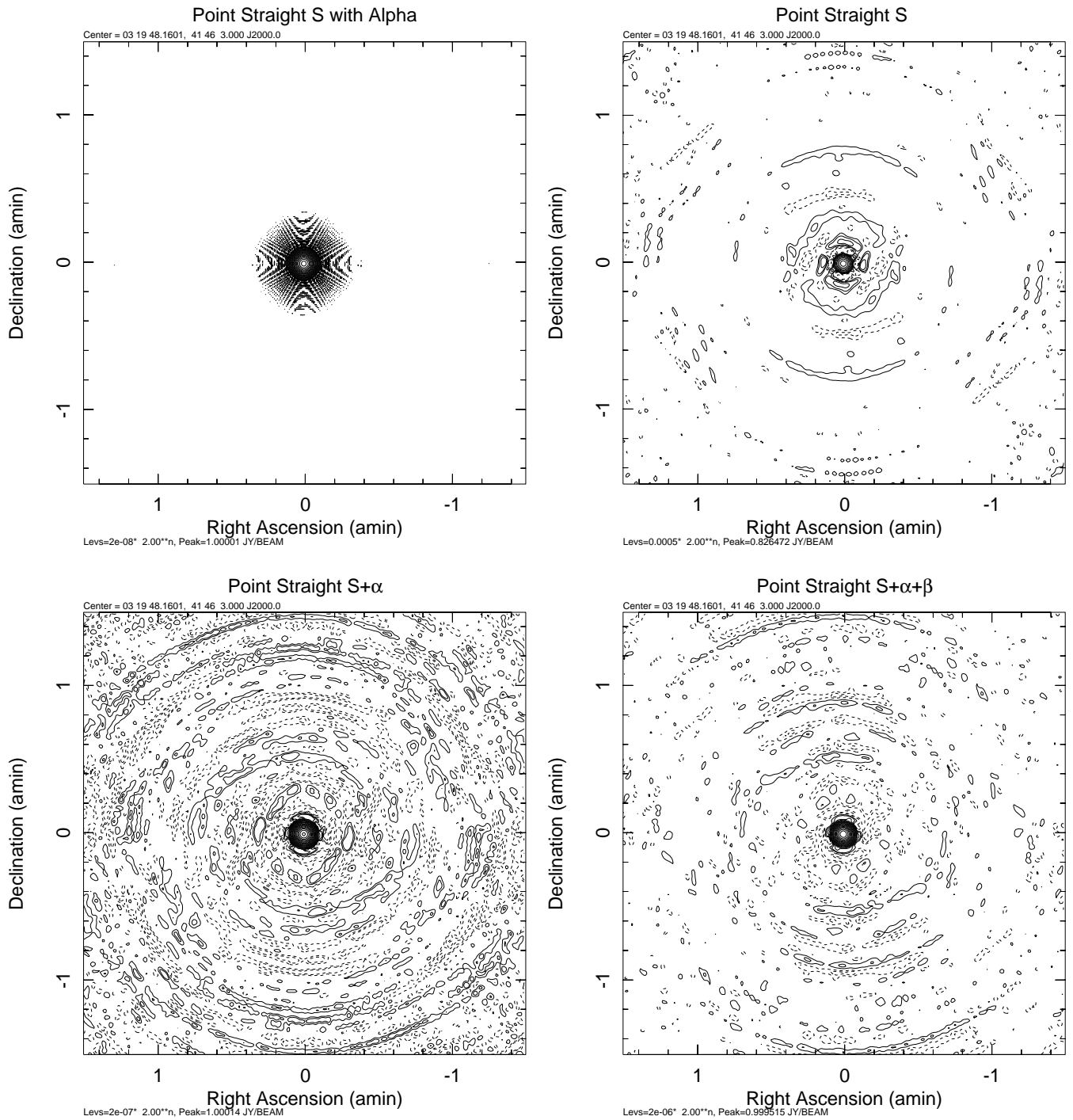


Fig. 3. Model 1.

Top left Imaged with Alpha=-0.7, norder=0; 285 CC Sum = 1.0 Jy, resid= 1.57×10^{-7} , -1.55×10^{-7} mJy RMS= 1.9×10^{-6} mJy/bm DR= 5.1×10^8 . Contour levels are powers of 2 from 2.0×10^{-5} mJy/beam, the peak in the image is 1.0 Jy/beam. Negative contours are dashed.

Top right Imaged with norder=0 154 CC Sum=0.865 resid=3.6,-4.5 mJy, RMS = 0.25 mJy DR = 3.3×10^3 . Contour levels are powers of 2 from 0.5 mJy/beam, the peak in the image is 0.8264 Jy/beam.

Bottom left Imaged with norder=1 271 CC sum=1.00013 Jy, resid= 1.9×10^{-3} , -1.6×10^{-3} mJy/bm, RMS= 2.0×10^{-4} mJy/bm, DR= 5.0×10^6 , center $\alpha = -0.7018$. Contour levels are powers of 2 from 2.0×10^{-4} mJy/beam, the peak in the image is 1.0 Jy/beam.

Bottom right Imaged with norder=2 362 CC sum=0.999582 Jy, resid= 1.4×10^{-1} , -1.0×10^2 mJy, RMS= 1.2×10^{-3} mJy, DR= 8.3×10^5 center $\alpha = -0.696$, $\beta = -0.013$ Contour levels are powers of 2 from 2.0×10^{-3} mJy/beam, the peak in the image is 1.0 Jy/beam.

TABLE II
Test Results

Test	Model	Fig	order	peak Jy/bm	Σ Jy/bm	Resid mJy/bm	σ mJy/bm	DR	Comments
1	1	3	0	1.000	1.000	1.6e-7,-1.6e-7	1.9e-6	5.1e8	Applied Alpha=-0.7
2	1	3	0	0.865	0.865	3.6,-4.5	0.25	3.3e3	
3	1	3	1	1.000	1.000	5.3e-3,-4.6e-3	2.0e-4	5.0e6	
4	1	3	2	1.000	1.000	0.14,-1.0e-2	1.2e-3	8.3e5	
5	2	4	0	0.810	0.900	4.6,-18.	0.30	2.7e3	
6	2	4	2	1.000	1.000	2.4e-4,-5.2e-5	1.3e-5	7.8e7	
7	3	5	0	0.053	0.438	0.16,-0.14	3.9e-2	1.4e3	ccfLim=0.85
8	3	5	1	0.076	0.547	0.20,-0.28	4.3e-2	1.8e3	OrdFlux=0.01, ccfLim=0.85
9	3	5	1	0.072	0.555	0.20,-1.0	3.6e-2	2.0e3	All solve for alpha
10	4	6	0	0.910	3.927	0.46,-0.51	6.1e-2	1.5e4	ccfLim=0.85
11	4	6	2	1.131	4.400	2.4,-2.5	0.38	3.0e3	ccfLim=0.7
12	5	7	1	1.000	1.577	0.34,-0.37	6.3e-2	1.2e3	
13	6	8	0	4.420	24.160	15.3,-21.7	2.1	2.1e3	
14	6	8	1	3.455	24.450	8.0,-8.8	1.2	2.9e3	
15	6	8	2	3.426	24.380	8.0,-8.9	1.2	2.9e3	
16	6	8	2	3.436	24.320	7.9,-8.9	1.1	3.2e3	

For the extended straight, steep spectrum source, solving for spectral index was only marginally better than ignoring it.

D. Model 4

This test was also of an extended source but offset from the origin. The source has a flattish spectrum of $\alpha=-0.05$ and a β of -0.1 and was a 5"×5" Gaussian of 4 Jy well separated from the origin. The first test (Figure 6 left) was imaging ignoring the spectrum. Due to the relatively flat spectrum, this worked relatively well with a sum of the CLEAN components of 3.927 Jy and a dynamic range of 14.8×10^3 .

The second test (Figure 6 right) was to solve for flux, α and β for residuals above 0.8 Jy, flux and α down to residuals of 0.3 Jy and only flux density below. The results became erratic solving for all terms for all residuals. The results were poor, the sum of the CLEAN flux density was 4.40 Jy, the α at the peak was -1.36 and the β was 0.87 with a dynamic range of 3.0×10^3 . Note, both plots in Figure 6 used the same contouring. For this test, solving for the spectrum resulted in MUCH worse results than ignoring the spectrum.

E. Model 5

This model was a double source using Model 1 and Model 3 with the latter offset from the center. The test on this model (Figure 7) solved for flux density and spectral index for all residuals. The result on the point source was good, with a peak of 1.0002 Jy and $\alpha=-0.704$ but the weaker extended source left strong artifacts and had a spectral index at the peak of -1.71. The total sum of CLEAN flux density was 1.577 Jy (model had 1.5 Jy) and the dynamic range was 1.6×10^4 . The dynamic range of the image is clearly limited by the extended source whose peak (0.075 Jy) is above the RMS by 1.2×10^3 . The presence of a poorly modeled extended source appears not to have affected the (good) result on the point source.

F. Model 6

This model contained components with a wide range of shapes, spectra and flux densities. The first test (Figure 8 upper left) is ignoring the spectra resulting in the expected poor results, a dynamic range of 2.1×10^3 . The dynamic range appears limited by the point sources, especially "H" in the north of the field.

The second test (Figure 8 upper right) was solving for flux density and α above 0.3 Jy and only flux density below resulting in a dynamic range of 2.9×10^3 . This was somewhat better than ignoring the spectra but the dynamic range is limited by artifacts from extended sources, especially component "K", also used in Model 4. There are no visible artifacts from the strong point sources.

The third test (Figure 8 lower left) was solving for flux density, α and β for residuals above 1.0 Jy; solving for flux density and α above 0.3 Jy and only flux density below. This produces an image very similar to that from the second test and also has a dynamic range of 2.9×10^3 . The similarity is likely the results of not solving for β for residuals on the extended sources.

The final test (Figure 8 lower right) on this model was to repeat the third test but using $ccLim=0.9$ to force very frequent re-computation of the residual images. This should inhibit any accumulating instability in the inner CLEAN component selection. Again the results are barely distinguishable from the second test with a slightly better dynamic range of 3.2×10^3 .

G. What went wrong?

The general theme of the tests presented is that this technique works very well for point sources reproducing well the input model but performs poorly to badly for resolved sources. Well into the CLEAN, solutions for higher order terms become increasingly erratic; however, reducing the order of the solution as the CLEAN progresses damps the worst instabilities but still produces mediocre results.

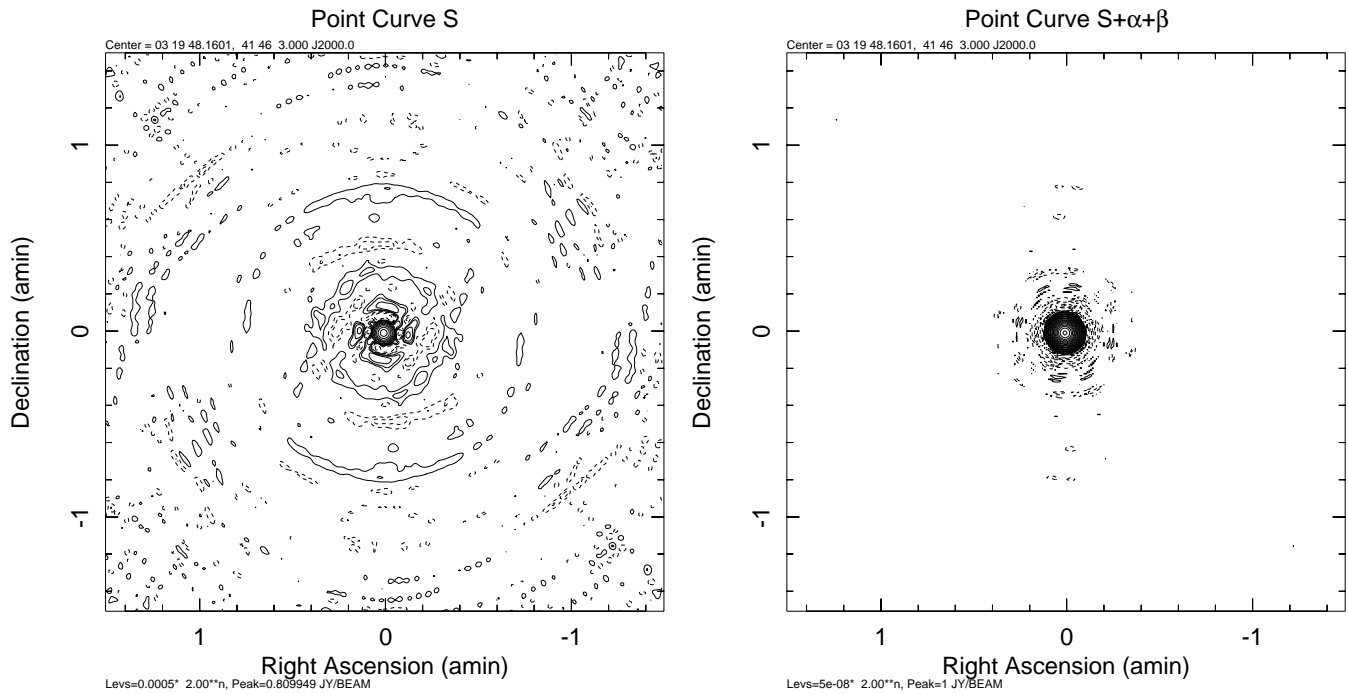


Fig. 4. Model 2.

Left Imaged with $norder=0$. 162 CC Sum=0.900499 Jy, resid=4.6, -18 mJy/beam, RMS=0.3 mJy/beam, DR= 2.7×10^3 . Contour levels are powers of 2 from 0.5 mJy/beam, the peak in the image is 0.81 Jy/beam.

Right Imaged with $norder=2$. 286 CC sum=0.999996 Jy, resid= 2.4×10^{-4} , -5.2×10^{-5} mJy/beam, RMS= 1.3×10^{-5} mJy, DR= 7.8×10^7 , center $\alpha=-0.69987$, $\beta=-0.2011$ Contour levels are powers of 2 from 5.0×10^{-8} mJy/beam, the peak in the image is 1.00 Jy/beam.

The spectra produced for resolved sources are much steeper than the input model and the resultant curvature has little relation to the model values. This points to a basic inability of the process to separate spectrum from structure as both will cause a variation of visibility with frequency for a given time-baseline sample. Further analysis of the problem in [8] revealed similar artifacts which were traced to the varying surface brightness sensitivity with frequency. These artifacts were eliminated when a frequency dependent taper was applied to give an approximately constant resolution with frequency. Such an approach might improve the performance of the technique presented here.

VII. CONCLUSION

A technique of solving for spectra in the image deconvolution process based on the Sault-Wieringa technique was presented and tested using simulated data with a variety of models. The technique was extended to second order allowing for solving for flux density, spectral index and spectral curvature. This worked well for point sources but gives very poor results on well resolved model components. This poor results on resolved components appears to be caused by an inability to separate source spectrum from structure.

ACKNOWLEDGMENT

The authors would like to thank Ed Fomalont for discussions on this topic.

REFERENCES

- [1] W. D. Cotton, "Towards a Wide-band Spectral Imaging Technique in Orbit," *Obit Development Memo Series*, vol. 3, pp. 1–10, 2008.
- [2] R. J. Sault and M. H. Wieringa, "Multi-frequency synthesis techniques in radio interferometric imaging," *Astron. Astrophys. Suppl.*, vol. 108, pp. 585–594, December 1994.
- [3] D. Fenech, I. Stewart, and S. Garrington, "Wide-band Imaging with e-Merlin," <http://www.ira.inaf.it/meetings/evn9/presentations/40-Garrington.pdf>, 2009.
- [4] W. D. Cotton, "Obit: A Development Environment for Astronomical Algorithms," *PASP*, vol. 120, pp. 439–448, 2008.
- [5] J. A. Högbom, "Aperture Synthesis with a Non-Regular Distribution of Interferometer Baselines," *Astron. Astrophys. Suppl.*, vol. 15, pp. 417–+, Jun. 1974.
- [6] F. R. Schwab, "Optimal Gridding of Visibility Data in Radio Interferometry," in *Indirect Imaging. Measurement and Processing for Indirect Imaging*. Australia, Cambridge University Press, Cambridge, England, New York, NY, L C # QB51.3.E43 I53 1984. ISBN # 0-521-26282-8. P.333, 1983, 1983, pp. 333–+.
- [7] W. D. Cotton, "Special problems in imaging," in *Synthesis Imaging in Radio Astronomy*, ser. ASP Conference Series, R. A. Perley, F. R. Schwab, and A. H. Bridle, Eds., no. 6. Astronomical Society of the Pacific, 1989, pp. 243–246.
- [8] W. D. Cotton, "High Dynamic Range Wide Bandwidth Imaging," *Obit Development Memo Series*, vol. 19, pp. 1–, 2010.

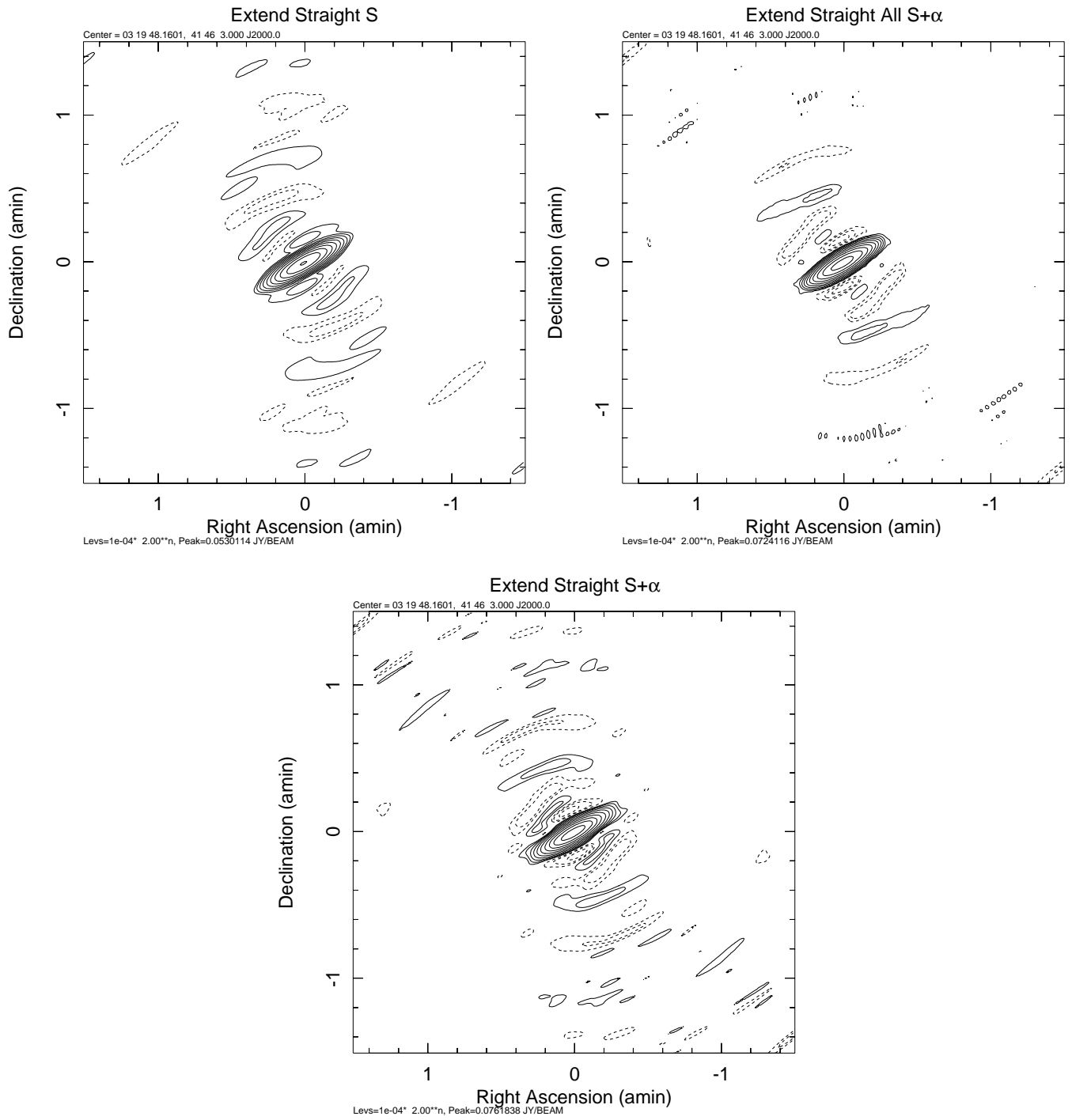


Fig. 5. Model 3.

Top left Imaged with norder=0 ccfLim=0.85. 2000 CC Sum = 0.43385 Jy, resid=0.16,-0.14 mJy, RMS= 3.89×10^{-2} mJy, DR= 1.4×10^3 . Contour levels are powers of 2 from 0.5 mJy/beam, the peak in the image is 0.053 Jy/beam.

Top right

Imaged with norder=1 for all, ccfLim=0.85 2000 CC Sum = 0.55475 resid=0.20, -1.0 mJy, RMS= 3.6×10^{-2} mJy DR= 2.0×10^3 Contour levels are powers of 2 from 0.1 mJy/beam, the peak in the image is 0.072 Jy/beam.

Bottom Imaged with norder=1 for OrdFlux=0.01; i.e. solved for α until residual reached 0.01, then only flux. Clean in order=1 for 167 CC, sum=0.356 Jy ccfLim=0.85. 2000 CC Sum = 0.54667 Jy, resid=0.20, -0.28 mJy, RMS= 4.3×10^{-2} mJy, DR= 1.8×10^3 . Contour levels are powers of 2 from 0.1 mJy/beam, the peak in the image is 0.076 Jy/beam.

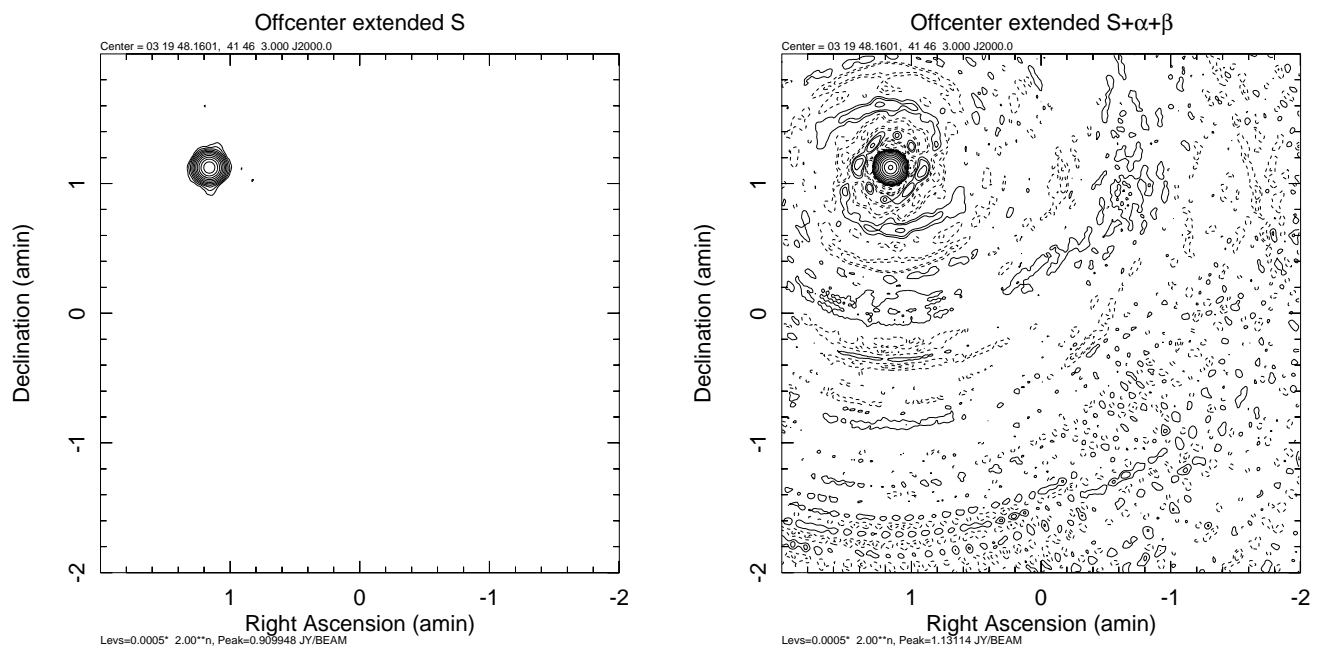


Fig. 6. Model 4.

Left Imaged with $n_{term} = 0$, $ccfLim=0.85$. 2000 CC Sum = 3.927 Jy resid = 0.46, -0.51 mJy, $RMS=6.13 \times 10^{-2}$ mJy DR = 14.8×10^3 . Contour levels are powers of 2 from 0.5 mJy/beam, the peak in the image is 0.9099 Jy/beam.

Right Imaged with $n_{term} = 2$, $OrdFlux=[0.3,0.8]$, $ccfLim=0.7$, 1000 CC, Sum = 4.39997 Jy, resid = 2.4, -2.5 mJy, $RMS=0.38$ mJy, DR = 3.0×10^3 . Contour levels are powers of 2 from 0.5 mJy/beam, the peak in the image is 1.131 Jy/beam.

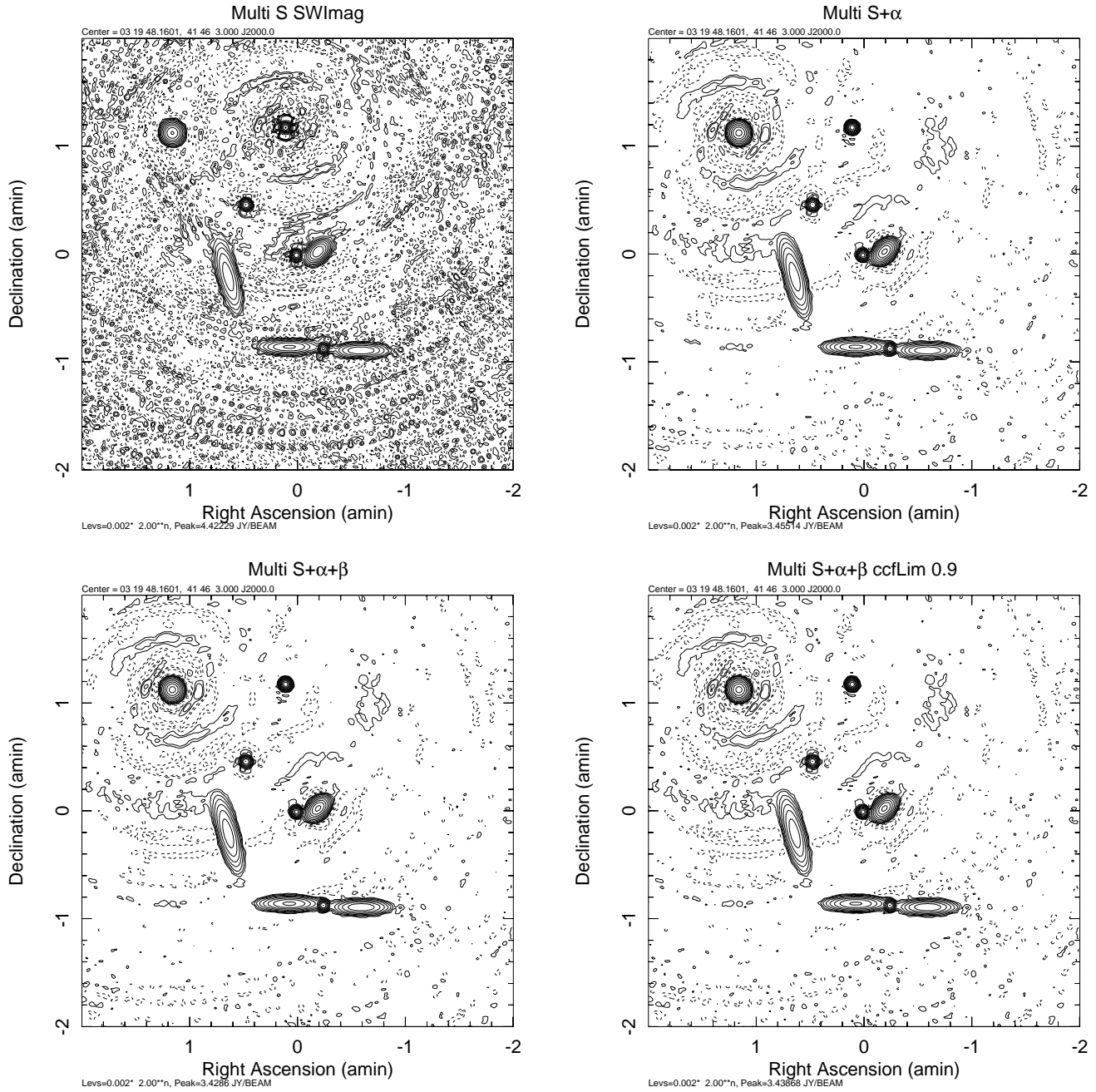


Fig. 8. Model 6.

Top left Imaged with $n_{\text{term}} = 0$, $\text{ccfLim}=0.7$ 5000 CC, Sum = 24.16 resid=0.0153,-0.0217 mJy/bm, RMS=2.1 mJy/bm, DR= 2.1×10^3 . Contour levels are powers of 2 from 2 mJy/beam, the peak in the image is 4.42 Jy/beam.

Top right Imaged with $n_{\text{term}} = 1$ OrdFlux=[0.3,1.0] 5000 CC Sum = 24.45 resid=8.0,-8.8 mJy/bm, RMS=1.21 mJy/bm DR= 2.9×10^3 , $\text{ccfLim}=0.7$. Contour levels are powers of 2 from 2 mJy/beam, the peak in the image is 3.455 Jy/beam.

Bottom left Imaged with $n_{\text{term}} = 2$ OrdFlux=[0.3,1.0], $\text{ccfLim}=0.7$, 5000 CC, Sum = 24.38 Jy, resid=7.96,-8.9 mJy/bm, RMS=1.19 mJy/bm, DR= 2.9×10^3 . Contour levels are powers of 2 from 2 mJy/beam, the peak in the image is 3.426 Jy/beam.

Bottom right Imaged with $n_{\text{term}} = 2$ OrdFlux=[0.3,1.0], $\text{ccfLim}=0.9$ 5000 CC, Sum = 24.32 Jy, resid=0.00793,-0.00887, RMS=1.07 mJy, DR= 3.2×10^3 Contour levels are powers of 2 from 2 mJy/beam, the peak in the image is 3.436 Jy/beam.